

Modelling heat transfer in flashing CO₂ fluid upon rapid decompression in pipelines

S. Brown, S. Martynov & H. Mahgerefteh

Department of Chemical Engineering, University College London, UK

Abstract

Accurate prediction of transient releases of CO₂ fluid from high-pressure transportation pipelines is important for the hazard assessment of such pipelines and the planning of their routine venting procedures. The accurate prediction of the fluid phase content, mass flow rate, pressure and temperature is key to the emergency response strategy or the vent pipe design, and is fundamental to the pipeline design and material selection for fracture control. Commonly to calculate releases of flashing fluids, such as hydrocarbons, from high-pressure vessels and pipelines, the simplifying assumption of a homogeneous equilibrium mixture (HEM) is applied. While this approach has proven to be robust for hydrocarbon mixtures, its validity is limited to inertia-dominant flows where the vapour and liquid-phases are well mixed. In the case of CO₂ fluid, the widely different densities of the vapour and liquid phases can lead to phase stratification in the pipeline during its decompression. The fluid phase stratification creates phase slip and thermal non-equilibrium between the phases, significantly impacting the outflow rate. In this work, a two-fluid compressible flow model is used to investigate the impact of thermal non-equilibrium on transient CO₂ pipeline decompression; the model predictions are compared with the results of simulations using HEM model as well as the experimental data on CO₂ releases from a large-scale pipeline.

Keywords: multi-phase flow, non-adiabatic flow, mathematical modelling, large-scale release experiment.

1 Introduction

Alongside renewable energy sources CO₂ Capture and Storage (CCS) is widely considered as a key technology in mitigating global CO₂ emissions, potentially



reducing the cost of inaction by some \$2 trillion over the next 40 years (IEA [1]). It is estimated by Element Energy [2] that transporting the predicted 2.3–9.2 Gt of captured CO₂ to its point of storage will require the use of a global network of between 95,000–550,000 km of pipeline by 2050.

For the transportation of such large amounts of CO₂ to be economical the majority of CCS pipelines will need to be operated in the dense or supercritical-phase rather than in the vapour-phase (Roussanaly *et al.* [3]). In Europe this will likely mean pipelines at line pressures above 100 bar passing through or near populated areas. Given that CO₂ is increasingly toxic at concentrations higher than 7% (Kruse and Tekiela [4]), the safety of CO₂ pipelines is of great importance and indeed pivotal to the public acceptability of CCS as a viable means for tackling the impact of global warming.

Central to assessing the safety of such pipelines is the accurate prediction of the decompression and the discharge rate of the escaping inventory in the event of accidental pipeline rupture. Such data forms the basis for determining the minimum safe distances to populated areas, emergency response planning and the optimum spacing of emergency shutdown valves.

The accurate modelling of the decompression process during pipeline rupture requires accounting for a number of complex and interacting phenomena. In particular, in the case of a volatile fluid such as dense-phase or supercritical CO₂, by far the biggest challenge is the correct modelling of the ensuing complex flow dynamics associated with the transition from single to two-phase flow.

In attempting to model the two-phase flow behaviour, the majority of pipeline depressurisation models reported in the literature have utilised the simplistic Homogeneous Equilibrium Mixture (HEM) model [5–7] where the constituent fluid phases are assumed to remain in thermal and mechanical equilibrium throughout the decompression process. Consequently, important phenomena, such as phase slip and non-equilibrium liquid/vapour transition, are ignored. As an alternative to the HEM the compressible two-fluid model (see for the general formulation [8, 9]) which has been widely used in the petroleum and nuclear industries [10, 11] is in principle capable of simulating the inter-phase dynamics and flow regimes of interest. Here, the dynamics of each phase are described independently; however, in order to account for the interactions between the phases, empirical models are required for the heat, mass and momentum transfer effects. Modelling the interfacial heat transfer and friction requires knowledge of the interfacial flow area, which in turn depends on the regime/ pattern of two-phase flow. Since the interfacial processes are difficult to measure there is a lack of validated correlations for closure of two-phase flow models. Most existing models have been developed for boiling and flashing flow of water (Bestion [10]), and hence their adaptation to CO₂ is uncertain. Furthermore, the heat transfer between the fluid, which cools during upon expansion, and the pipe wall may significantly affect the fluid temperature and the rate of release in case of small punctures (Martynov *et al.* [12]). Hence, the heat exchange between the two-phase flow and the pipe wall also needs to be accurately described in the flow model.



In this work the compressible two-fluid model is applied to simulate the decompression of CO₂ following pipeline failure. In the absence of dedicated empirical correlations for CO₂ relatively simple constitutive relations available in the literature are employed to account for inter-phase heat, mass and momentum exchanges. This model is coupled with a transient heat conduction model to simulate the heat transfer between the fluid and pipe wall. The sensitivity of the model's predictions to these effects is investigated based on parametric studies. The predictions obtained are compared against the measured decompression test data recorded for a CO₂ pipeline rupture test conducted as part of the FP7 project [13].

2 Theory

2.1 Two-fluid model

The rigorous description of transient flow during the decompression of compressible two-phase flow requires equations accounting for the behaviour of each constituent phase (see for example Ishii and Hibiki [9]). Accordingly, in this work the single pressure two-fluid model (see for example Stewart and Wendroff [8]) is applied to the two-phase flow of CO₂. This model may be written in the general form (see for example Paillere *et al.* [14]):

$$\frac{\partial \mathbf{U}}{\partial t} + \frac{\partial \mathbf{F}(\mathbf{U})}{\partial x} = \mathbf{C}^{nv} + \mathbf{C}^v + \mathbf{S}, \quad (1)$$

where

$$\mathbf{U} = \begin{pmatrix} \alpha_v \rho_v \\ \alpha_l \rho_l \\ \alpha_v \rho_v u_v \\ \alpha_l \rho_l u_l \\ \alpha_v \rho_v E_v \\ \alpha_l \rho_l E_l \end{pmatrix}, \quad \mathbf{F}(\mathbf{U}) = \begin{pmatrix} \alpha_v \rho_v u_v \\ \alpha_l \rho_l u_l \\ \alpha_v \rho_v u_v^2 + \alpha_v P \\ \alpha_l \rho_l u_l^2 + \alpha_l P \\ \alpha_v \rho_v u_v H_v \\ \alpha_l \rho_l u_l H_l \end{pmatrix}, \quad (2)$$

u_k , ρ_k , E_k and H_k are respectively the velocity, density, total energy and specific total enthalpy for each phase k . P is the system pressure, while α_k are the volume fractions for which the following relation holds:

$$\alpha_v + \alpha_l = 1, \quad (3)$$



\mathbf{C}^{nv} and \mathbf{C}^v are the vectors of non-viscous differential terms and viscous non-differential terms respectively. These in turn are given by:

$$\mathbf{C}^{nv} = \begin{pmatrix} 0 \\ 0 \\ P \frac{\partial \alpha_v}{\partial x} + F_v^{nv} \\ P \frac{\partial \alpha_l}{\partial x} + F_l^{nv} \\ -P \frac{\partial \alpha_v}{\partial t} + u^{int} F_v^{nv} \\ -P \frac{\partial \alpha_l}{\partial t} + u^{int} F_v^{nv} \end{pmatrix}, \quad \mathbf{C}^v = \begin{pmatrix} 0 \\ 0 \\ F_v^v \\ F_l^v \\ 0 \\ 0 \end{pmatrix}, \quad (4)$$

where u^{int} , F_k^{nv} and F_k^v are respectively the interfacial velocity, inter-phase forces containing derivative terms and viscous friction terms.

Finally \mathbf{S} is the vector of non-differential source terms (such as gravity and phase change) given by:

$$\mathbf{S} = \begin{pmatrix} \Gamma_v \\ \Gamma_l \\ u^{int} \Gamma_v + F_v^D + \alpha_v \rho_v g_x \\ u^{int} \Gamma_l + F_l^D + \alpha_l \rho_l g_x \\ u^{int} F_v^D + H_l \Gamma_v + q_v^i + \frac{4q_v^w}{D_h} + \alpha_v \rho_v u_v g_x \\ u^{int} F_l^D + H_v \Gamma_l + q_l^i + \frac{4q_l^w}{D_h} + \alpha_l \rho_l u_l g_x \end{pmatrix}, \quad (5)$$

where Γ_k , F_k^D , H_i , q_k^i and q_k^w are respectively the mass transfer flux, the inter-phase drag force, specific total enthalpy and heat exchanged with the interface (i) and the wall (w) for phase k . D_h is the internal diameter of the pipe and g_x is the projection of the gravity vector onto the x -coordinate axis.

2.2 Constitutive relations

It is well known (Stuhmiller [15]) that the two-fluid model is non-hyperbolic in the case $F_k^{nv} = 0$. Whence we follow the commonly used approach of applying the interfacial pressure correction force [15]:

$$F_k^{nv} = (P^{int} - P) \frac{\partial \alpha_k}{\partial x}, \quad (6)$$

where

$$P^{int} = P - \sigma \frac{\alpha_v \rho_v \alpha_l \rho_l}{\alpha_v \rho_l + \alpha_v \rho_l} (u_v - u_l)^2, \quad (7)$$

values of $\sigma \geq 1$ enforce hyperbolicity. For the purposes of this work $\sigma = 2$ is used.



u^{int} is defined by the weighted average of the vapour and liquid velocities:

$$u^{int} = \alpha_v u_v + (1 - \alpha_v) u_l. \quad (8)$$

Following Cortes [16], the inter-phase drag terms F_k^D are defined by:

$$F_v^D = -F_l^D = C_f \alpha_v^m \alpha_l^n (\kappa_l \rho_l + \kappa_v \rho_v) |v_v - v_l| (v_v - v_l). \quad (9)$$

where C_f , m , n , κ_l and κ_v are the friction coefficient and flow regime dependent coefficients respectively. m and n are both unity, while $\kappa_l = 0.752$ and $\kappa_v = 0.01063$. The viscous friction terms are given by:

$$F_v^v = -\frac{2f \alpha_v \rho_v |v_v| v_v}{D_h} \quad (10)$$

and

$$F_l^v = -\frac{2f \alpha_l \rho_l |v_l| v_l}{D_h}, \quad (11)$$

where f is the Fanning friction factor, which is assumed to take the constant value of 0.017 (Garcia-Cascales *et al.* [17]).

The q_k^i are taken to be:

$$q_v^i = \frac{C_\tau}{\tau} \alpha_v \alpha_l (h_{sat,v} - h_v) \quad (12)$$

$$q_l^i = \frac{C_\tau}{\tau} \alpha_v \alpha_l (h_{sat,l} - h_l) \quad (13)$$

where C_τ and τ are problem specific constants and the subscript *sat* indicates saturated properties. We use $C_\tau = 1$ throughout.

The above q_k^i are used to define the mass transfer fluxes:

$$\Gamma_v = -\Gamma_l = -\frac{(q_v^i + q_l^i)}{h_{sat,v} - h_{sat,l}}. \quad (14)$$

The q_k^w are then defined as:

$$q_k^w = \eta_k \alpha_k (T_w - T_k) \quad (15)$$

where T_k and T_w are respectively the temperature for phase k and the temperature of the wall at the interior boundary.

Given the highly turbulent flow during depressurisation, we assume that only forced convective heat transfer occurs between both the flowing liquid and vapour phases and the inner pipe wall. Accordingly, the corresponding heat transfer coefficient, η is calculated using the Dittus–Boelter correlation [18]:

$$\eta_k = 0.023 Re_k^{0.8} Pr_k^{0.4} \frac{k_k}{(\alpha_k D_h)}, \quad (16)$$

where k_k , Re_k and Pr_k are the thermal conductivity, Reynold's number and Prandtl's number for each phase k respectively.



2.3 Heat conduction in pipe wall

In order to calculate the instantaneous heat flux, q_w and the temperature of the wall, T_w must be calculated. To accomplish this the transient heat conduction equation for a two-dimensional cross section of the pipe wall (in cylindrical coordinates) is solved:

$$\frac{\partial T_w}{\partial t} = \frac{k_w}{\rho_w c_{p,w}} \left(\frac{1}{r} \frac{\partial}{\partial r} \left(r \frac{\partial T_w}{\partial r} \right) + \frac{\partial^2 T_w}{\partial x^2} \right), \quad (17)$$

where k_w , ρ_w and $c_{p,w}$ are respectively the pipe wall thermal conductivity, density and heat capacity and are assumed to take the constant values $53.65 \text{ W m}^{-1} \text{ K}^{-1}$, 7850 kg m^{-3} and $460 \text{ J kg}^{-1} \text{ K}^{-1}$ representative of carbon steel (Perry and Green [19]). r , is the radial coordinate. Equation (17) is solved numerically using a explicit, central difference method (Pletcher *et al.* [20]).

For simplicity, the pipe wall is assumed to be perfectly insulated so that the heat exchange with the surroundings may be ignored.

3 Results and discussion

The following describes the application of the model described above to a Full Bore Rupture (FBR) CO₂ pipeline release experiment conducted as part of the FP7 funded CO2PipeHaz project [13]. The experiment utilised a fully instrumented 256 m long, 233 mm i.d. and 20 mm wall thickness pipeline made of 16 Mn Carbon Steel with a maximum safe operating pressure of 200 bara [12].

The study is conducted to investigate the impact of the flow model's constitutive parameters on the simulated in-pipe transient pressure and temperatures during the pipeline decompression as compared to the recorded data. In particular, the effects of thermal relaxation time (τ) and fluid/pipe wall heat exchange are investigated. For the sake of comparison, the corresponding predictions using the HEM model [6] are also presented.

Prior to rupture, the pipeline is filled with *ca.* 6.5 tonnes of CO₂ containing 0.2% vol./vol. at saturation conditions 36 bara and 274 K corresponding to a vapour fraction $\alpha_v = 0.5$. The ambient pressure is 1 bara.

The simulations are performed using a spatial discretisation with two levels of refinement, the coarsest level containing 100 cells, with a CFL number of 0.3. The heat exchange between the pipe and the surroundings is considered negligible given that the pipe is thermally insulated. The physical properties of both the liquid and vapour-phases are computed using the Peng–Robinson equation of state [21]. Unless otherwise stated the thermal relaxation time, τ and inter-phase friction coefficient, C_f are taken as $\tau = 5 \times 10^{-5}$ s and unity respectively.

3.1 Influence of thermal relaxation time

Figures 1(a) and (b) respectively show the predicted variation of pressure with time at transducers P3 (10.4 m from the rupture plane) and P8 (139.5 m from



the rupture plane) following FBR for thermal relaxation times, τ ranging from 5×10^{-6} to 5×10^{-4} s. Also shown in the same figure are the corresponding recorded experimental data and the HEM model (i.e. $\tau, C_f \rightarrow 0$) predictions.

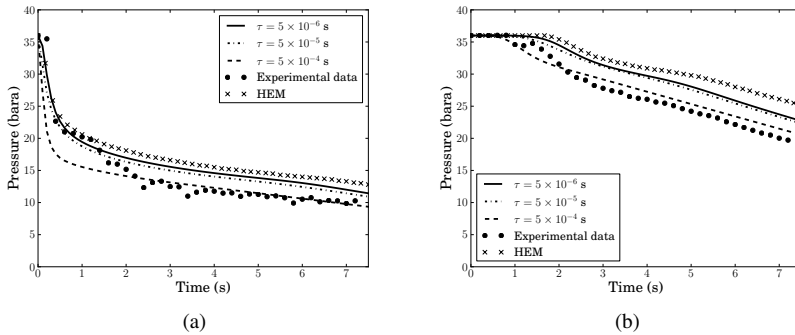


Figure 1: Variation of the fluid pressure at P3 (a) and P8 (b) with time following the initiation of decompression. Predicted using the HEM and the two-fluid model with various thermal relaxation times (τ) and the experimental data.

As may be observed from the data in Figure 1(a) the experimental data show three distinct trends. In order of appearance these include:

1. an initial pressure plateau corresponding to the time taken for the decompression wave to reach the pressure transducer;
2. a rapid pressure drop corresponding to the arrival of the decompression wave followed by a second pressure plateau;
3. a relatively slow depressurisation rate commencing with the passage of the decompression wave from the transducer location.

From Figure 1(a) (transducer P3) it can be seen that the simulations capture the initial rapid decline in the measured pressure during the first *ca.* 0.5 s following depressurisation. Lower pressure drops are observed as the relaxation time decreases, with the case $\tau = 5 \times 10^{-5}$ s showing the best agreement with the experimental data. Post *ca.* 0.5 s corresponding to the slower pressure decay region, the degree of agreement with the experimental data improves as the relaxation time increases, with HEM producing the worst predictions. Similar trends in the data may be observed in Figure 1(b), albeit at a slower depressurisation rate.

The above observations suggest that non-equilibrium effects become more important with the passage of time and distance from the rupture plane.

Figures 2(a) and (b) respectively show comparisons of the predictions of the liquid and vapour temperatures with experimental recorded thermocouple T4 (10.4 m from the rupture plane) respectively. As may be observed, the measured

temperature profiles show similar trends to the pressure data (see Figures 1(a) and (b)). The initial rapid temperature drop is followed by a decline in the rate of cooling. Also, as in the pressure data, a short duration plateau (*ca.* 0.5 s) in the measured temperature at the beginning of the depressurisation may be observed. As expected, the vapour-phase exhibits a slightly greater degree of cooling.

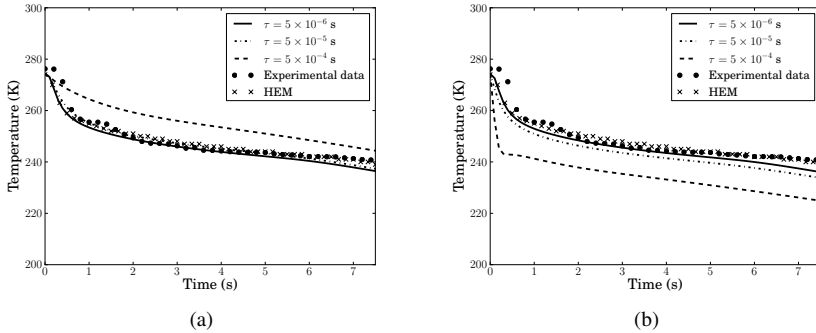


Figure 2: Variation of the temperature in liquid (a) and vapour (b) phases at T4 with time following the initiation of decompression. Predicted using the HEM and the two-fluid model with various thermal relaxation times (τ) and the experimental data.

For both the liquid and vapour-phases, the longest relaxation time of $\tau = 5 \times 10^{-4}$ s produces the worst agreement with the recorded temperatures. For all the relaxation times, relatively good agreement may be observed between theory and experiment with little discernable differences in model performance.

To elucidate the phase behaviour during the depressurisation, Figure 3 shows the thermodynamic trajectory of the CO₂ decompression at the collocated pressure transducer-thermocouple pair P3 and T4, relative to the CO₂ saturation line. Also shown are the trajectories of the liquid-phase obtained from the simulations presented above. As can be seen the experimental data shows three distinct trends:

1. a nearly isothermal pressure drop of *ca.* 20 bara from the initial state accompanied by a temperature drop of less than 4 K. This results in the fluid falling into the meta-stable region for the liquid content of the mixture;
2. a temperature drop from *ca.* 274 K to 257 K, i.e. almost the saturation temperature, at constant pressure;
3. finally, the decompression continues parallel to the saturation line.

The predictions using $\tau = 5 \times 10^{-4}$ s produce a reasonable approximation of the first of these trends which, with reference to Figure 1(a), occurs in under *ca.* 0.3 s. The results obtained with $\tau = 5 \times 10^{-5}$ s diverge visibly from the saturation line, while those using $\tau = 5 \times 10^{-6}$ s as well as the HEM model both remain on the saturation line throughout. This comparison shows that the HEM is

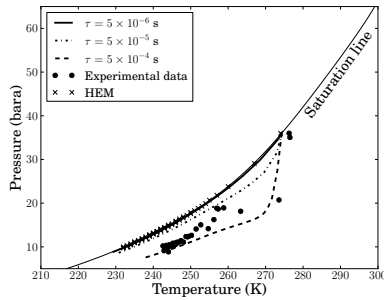


Figure 3: Thermodynamic trajectories during decompression at P3-T4 relative to saturation line of CO₂.

incapable of producing reasonable predictions for this scenario, as the departure from thermodynamic equilibrium is too great for the flow to be approximated accurately.

3.2 Fluid/pipe wall heat transfer

In the pipeline rupture release experiments, although the pipe wall was insulated, and hence did not exchange heat with the surrounding, the initially warm steel pipe wall represented a significant source of heat. To simulate the impact of heat exchange between the flowing fluid and the pipe wall during the decompression, the flow model was coupled with the transient pipe wall heat conduction model described in Section 2.3. Prior to initiation of the release, the pipe wall is assumed to be in thermal equilibrium with the fluid. For the numerical solution of the heat conduction equation the pipe wall is discretised using an orthogonal mesh with the nodes at the internal wall collocated with those used for the fluid calculations.

Figures 4(a) and (b) show the comparison of the liquid and vapour-phase temperature predictions assuming adiabatic flow and those obtained accounting for pipe wall/fluid heat transfer model at T4 (10.4 m from rupture plane) against experimental data. As may be observed, in all cases, there is good accord between theory and experiment with no discernible difference in the predictions by the models accounting for and ignoring heat transfer with the pipe wall. Also, as expected, at any given time during the depressurisation process, the liquid temperature predicted by the non-adiabatic model is higher than that based on the adiabatic model.

4 Conclusion

In this paper a non-equilibrium two-phase model describing fully compressible transient vapour-liquid flow was developed for the depressurisation of high pressure CO₂ pipelines. The model accounted both for phase slip and delayed



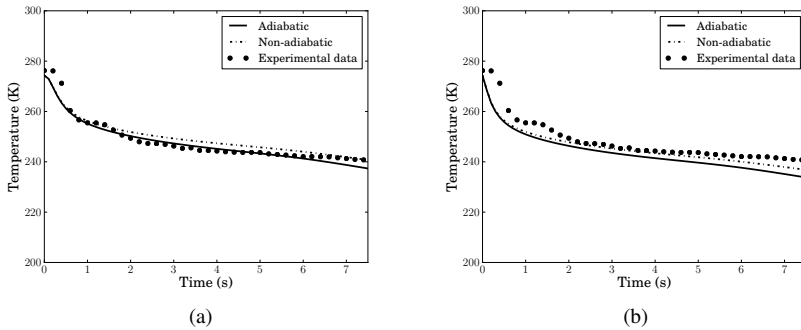


Figure 4: Variation of the temperature in liquid (a) and vapour (b) phases at T4 with time following the initiation of decompression predicted with adiabatic and non-adiabatic models and the experimental data.

phase transitions, and incorporated a cubic equation of state for the accurate prediction of pertinent fluid thermodynamic properties. The performance of the model was investigated by comparison with pressure and temperature data measured in a large-scale CO_2 pipeline decompression test as well as those predicted using the simplified HEM.

Given the uncertainty about the applicability of existing non-equilibrium two-phase models for flashing CO_2 flows, the phase interaction terms including friction and heat and mass transfer were modelled using simple constitutive relations, assuming a constant thermal relaxation time and inter-phase drag coefficient. Similarly, the fluid/pipe wall heat transfer was assumed to be via forced convection. It was shown that the predictions obtained were in reasonably good agreement with the experimental data, but were strongly dependent on the thermal relaxation time, which characterises the rate of inter-phase heat and mass transfer. In particular, better agreement between predictions and the measured pressures was obtained with increasing thermal relaxation time during the later stages of the depressurisation. Interestingly however, at the location closest to the release end of the pipe, for the initial *ca.* 1 s of the decompression, the smallest relaxation time produced the best agreement. This transition had a more significant impact on the temperature predictions where, due to a sudden drop in the temperature, the predictions with the higher thermal relaxation time were found to be the least accurate.

The coupling of the models for the fluid flow with that for the heat conduction in the pipe wall had only a small impact on the results close to the open end of the pipeline, which is characterised by low temperatures and high fluid velocities in this region. For longer duration releases, once the pressure gradients have been reduced, the thermal interaction between the fluid and pipe wall can be expected to have a more substantial effect on the decompression.

In summary, the predictions obtained from the two-fluid non-equilibrium model show better agreement with the experimental data in comparison with the commonly used HEM model. The latter was found to provide reasonable predictions only for the first 0.5 s of the decompression process and close to the release plane (for the case presented, within 30 m of the rupture plane).

Furthermore, the simulations presented in this work were for Full Bore Rupture, where the two-phase flow is expected to be closer to homogeneous equilibrium behaviour as compared to pipeline puncture. Here the slower flow rate along with the more confined expansion through the puncture aperture will result in phase slip and delayed phase disengagement.

Acknowledgements

This work was supported by the UK Engineering and Physical Science Research Council (EPSRC reference EP/K000446/1) and the European Union 7th Framework Programme FP7-ENERGY-2012-1-2STAGE under grant agreement number 309102.

References

- [1] IEA, Energy technology perspectives 2012: Pathways to a clean energy system, 2012.
- [2] Element Energy, CO₂ pipeline infrastructure: An analysis of global challenges and opportunities. Technical report, Final report for IEA Greenhouse Gas programme, 2010.
- [3] Roussanaly, S., Bureau-Cauchois, G. & Husebye, J., Costs benchmark of CO₂ transport technologies for a group of various size industries. *International Journal of Greenhouse Gas Control*, **12**, pp. 341–350, 2013.
- [4] Kruse, H. & Tekiela, M., Calculating the consequences of a CO₂-pipeline rupture. *Energy Conversion and Management*, **37(95)**, pp. 1013–1018, 1996.
- [5] Terenzi, A., Influence of real-fluid properties in modeling decompression wave interacting with ductile fracture propagation. *Oil & Gas Science and Technology*, **60(4)**, pp. 711–719, 2005.
- [6] Mahgerefteh, H., Brown, S. & Denton, G., Modelling the impact of stream impurities on ductile fractures in CO₂ pipelines. *Chemical Engineering Science*, **74**, pp. 200–210, 2012.
- [7] Popescu, M., Modeling of fluid dynamics interacting with ductile fraction propagation in high pressure pipeline. *Acta Mechanica Sinica*, **25(3)**, pp. 311–318, 2009.
- [8] Stewart, H.B. & Wendroff, B., Two-phase flow: Models and methods. *Journal of Computational Physics*, **56(3)**, pp. 363–409, 1984.
- [9] Ishii, M. & Hibiki, T., *Thermo-fluid Dynamics of Two-Phase Flow*. Smart Energy Systems, Springer: NY, 2006.



- [10] Bestion, D., The physical closure laws in the CATHARE code. *Nuclear Engineering and Design*, **124(3)**, pp. 229–245, 1990.
- [11] Bendiksen, K.H., Maines, D., Moe, R. & Nuland, S., The dynamic two-fluid model OLGA: theory and application. *Production*, **6(6)**, pp. 171–180, 1991.
- [12] Martynov, S., Brown, S. & Mahgerefteh, H., Modelling three-phase releases of carbon dioxide from high-pressure pipelines. *Process Safety and Environmental Protection*.
- [13] CO2PipeHaz. <http://www.co2pipehaz.eu/index.php>, 2012. [Online]. [Accessed on 5 July 2012].
- [14] Paillere, H., Corre, C. & Garcia Cascales, J., On the extension of the AUSM+ scheme to compressible two-fluid models. *Computers & Fluids*, **32(6)**, pp. 891–916, 2003.
- [15] Stuhmiller, J., The influence of interfacial pressure forces on the character of two-phase flow model equations. *International Journal of Multiphase Flow*, **3(6)**, pp. 551–560, 1977.
- [16] Cortes, J., On the construction of upwind schemes for non-equilibrium transient two-phase flows. *Computers & Fluids*, **31(2)**, pp. 159–182, 2002.
- [17] Garcia-Cascales, J.R., Mulas-Pérez, J. & Paillère, H., Advances in the Characterization of Transient Two-Phase Flow. *AIAA Journal*, **45(10)**, pp. 2579–2584, 2007.
- [18] Dittus, F. & Boelter, L., *Heat Transfer in Automobile Radiators of the Tubular Type*. University of California publications in engineering: University of California, University of California Press, 1930.
- [19] Perry, R.H. & Green, D.W., *Perry's Chemical Engineers' Handbook (7th Edition)*, 1997.
- [20] Pletcher, R., Tannehill, J. & Anderson, D., *Computational Fluid Mechanics and Heat Transfer, Second Edition*. Series in Computational and Physical Processes in Mechanics and Thermal Sciences, Taylor & Francis, 1997.
- [21] Peng, D.Y. & Robinson, D.B., A new two-constant equation of state. *Industrial & Engineering Chemistry Fundamentals*, **15(1)**, pp. 59–64, 1976.

